



# Anti-Flatness and Non-Local Magic in Two-Particle Scattering Processes

Caroline E. P. Robin <sup>\*</sup>

*Fakultät für Physik, Universität Bielefeld, D-33615, Bielefeld, Germany and*

*GSI Helmholtzzentrum für Schwerionenforschung, Planckstraße 1, 64291 Darmstadt, Germany*

Martin J. Savage <sup>†</sup>

*InQubator for Quantum Simulation (IQUS), Department of Physics,  
University of Washington, Seattle, WA 98195, USA.*

(Dated: October 28, 2025)

Non-local magic and anti-flatness provide a measure of the quantum complexity in the wavefunction of a physical system. Supported by entanglement, they cannot be removed by local unitary operations, thus providing basis-independent measures, and sufficiently large values underpin the need for quantum computers in order to perform precise simulations of the system at scale. Towards a better understanding of the quantum-complexity generation by fundamental interactions, the building blocks of many-body systems, we consider non-local magic and anti-flatness in two-particle scattering processes, specifically focusing on low-energy nucleon-nucleon scattering and high-energy Møller scattering. We find that the non-local magic induced in both interactions is four times the anti-flatness (which is found to be true for any two-qubit wavefunction), and verify the relation between the Clifford-averaged anti-flatness and total magic. For these processes, the anti-flatness is a more experimentally accessible quantity as it can be determined from one of the final-state particles, and does not require spin correlations. While the Møller experiment at the Thomas Jefferson National Accelerator Facility does not include final-state spin measurements, the results presented here may add motivation to consider their future inclusion.

arXiv:2510.23426v1 [quant-ph] 27 Oct 2025

---

<sup>\*</sup> [crobin@physik.uni-bielefeld.de](mailto:crobin@physik.uni-bielefeld.de)

<sup>†</sup> [mjs5@uw.edu](mailto:mjs5@uw.edu); On leave from the Institute for Nuclear Theory.

## I. INTRODUCTION

Understanding the complexity of quantum many-body systems is key to progress in an array of research and technology domains, including in accelerating future simulations using quantum computers. To that aim, techniques quantifying the quantum complexity, and hence classical computational hardness of simulating such systems, both modest-sized and at scale, continue to improve, driven in part by challenges facing classical computation and the development of quantum computers. One challenging area for classical simulations, in general, is predicting the properties and dynamics of matter under extreme conditions. They are plagued by sign problems, both in finding low-lying states at finite density and in their real-time evolution. Understanding how various aspects of complexity are generated by fundamental forces, and how they evolve in few-body and many-body environments is key towards better understanding the role of quantum information in these physical phenomena and designing resource-efficient simulation strategies.

The role of entanglement – which characterizes one aspect of quantum complexity – has been investigated in various areas of high-energy physics (HEP) and nuclear physics (NP). For example, building on the work of Ref. [1, 2] which identified maximum entanglement in Standard Model scattering processes, the suppression of fluctuations in entanglement from the S-matrix has been connected to the emergence of global symmetries beyond those explicit in the Lagrange density [3–7]. These are consistent with the results obtained from the large- $N_c$  limit of QCD [8], and extend to larger  $SU(N)$  spin-flavor symmetry groups [3, 9], consistent with the results of lattice QCD calculations [10]. This concept has also been applied in other settings, such as the Higgs sector of the Standard Model [11, 12], bosonic field theories [13], and higher-spin systems [14]. The maximum entanglement discussion of Ref. [1, 2] has been recently extended to perturbative gluon-gluon scattering in quantum chromodynamics [15]. Various studies of entanglement in few-nucleon scatterings [16–23], and in many-body nuclear systems [24–41] have also followed.

Quantum complexity beyond entanglement, in particular non-stabilizerness [42, 43], or “quantum magic” [44], is now being considered in an array of physical systems. The non-stabilizerness in a wavefunction is a measure of how much it differs from one that can be prepared efficiently classically, either as a measure of the distance to the nearest stabilizer state, or the number of such contributing states. As such, non-stabilizerness can provide guidance for partitioning simulations between classical and quantum hardware, both in the NISQ and fault-tolerant regimes. The recent development of practically-computable measures of non-stabilizerness based on Stabilizer Rényi Entropies (SREs) [46–50] have triggered a wide range of works investigating magic in various aspects of few-body and many-body structure and dynamics. In HEP and NP, this includes studies of magic in the dynamics of neutrino systems [51], in thermalization in gauge theories [52], in simulations of lattice gauge theories [53], in high-energy particle production [54, 55] and scattering [56–58], in nuclear and hyper-nuclear forces [59], in many-body nuclear models [60] and atomic nuclei [41]. These studies constitute efforts towards better understanding the role of quantum complexity in physical behaviors and designing optimal simulation strategies <sup>1</sup>.

Entanglement or magic alone, however, do not reflect the full complexity of a quantum state. This is because states with both large magic and low entanglement, and those with large entanglement and low magic can be prepared efficiently with classical resources. However, this becomes increasingly difficult as the entanglement or magic increases, respectively. Therefore it is the interplay between these two aspects that drive quantum complexity, and the need for quantum computers [62, 63]. Recently it has been put forward that this interplay is captured by the non-local magic [62] – the magic that cannot be removed from the system via local operations – and thus large non-local magic will be the key feature of quantum systems that drive future quantum advantages [44, 61, 64–84]. In holography theory, non-local magic has been shown to be responsible for gravitational back reaction and necessary for creating patterns of multipartite entanglement [62]. Non-local magic has also been studied in the transverse-field Ising model [82], and a similar concept has been studied in relation to the phases of matter [85].

One issue in accessing non-local magic is that it requires minimization under local operations, which quickly becomes computationally demanding. On the other hand, it has recently been established that the anti-flatness of the bi-partite entanglement spectrum of a state, which is related to the total magic [86, 87], can also partly capture the entanglement-magic interplay [63] and provide a lower bound to the non-local magic [62]. Anti-flatness has been explored in a number of systems [88], including the detection of phase transitions [89], in scrambling [90], and in the thermalization of non-Abelian gauge field theories [52].

In this work, we consider the role of anti-flatness and non-local magic in two-body scattering processes, specifically low-energy nucleon-nucleon scattering and high-energy Møller scattering. While these systems do not present

---

<sup>1</sup> The number of non-Clifford gates required to prepare a quantum state has been shown to be lower-bounded by the magic in that state. However, a strict relation remains to be established [46, 61].

challenges from a computational standpoint, they probe the potential capabilities of these fundamental processes to drive the quantum complexity of larger many-body systems. Previously, it has been shown that the Clauser-Horne-Shimony-Holt (CHSH) inequality can be violated in polarized Møller scattering [91], building on some of their previous works, e.g., Ref. [92]. Given the simplicity of two-particle systems, along with the fact that anti-flatness of the system can be recovered from measurements performed on one of the particles, we propose that polarized measurements performed on one of the final state particles from a set of specifically prepared polarized initial states are sufficient to reveal the changes in quantum complexity imparted by fundamental forces. Interestingly, it has recently been shown [88] that violations of the CHSH inequality depend upon the presence of local magic, but are suppressed by the presence of non-local magic.

## II. ANTI-FLATNESS AND NON-LOCAL MAGIC

The most general wavefunction of a system of two spin- $\frac{1}{2}$  particles (mapped to qubits),  $|\psi\rangle$ , requires the universal quantum gate set to prepare it from an arbitrary (classical) tensor-product state. The vector of matrix elements of the 16 generalized Pauli operators formed from  $\bar{\sigma} \in \{\hat{X}, \hat{Y}, \hat{Z}, \hat{I}\}$ ,  $\hat{P}_{ij} = \bar{\sigma}_i \otimes \bar{\sigma}_j$ , defines the  $\Xi_P$  values

$$\Xi_P = c_P^2/d, \quad c_P = \langle \psi | \hat{P} | \psi \rangle, \quad (1)$$

where  $d = 2^2$  and  $\sum_P \Xi_P = 1$ . If  $|\psi\rangle$  is a stabilizer state, it can be prepared efficiently using classical resources (using Clifford gates), and only  $d$  of the  $d^2$  quantities  $\Xi_P$  are non-zero, with values  $\Xi_P = 1/d$ , such that  $\xi = d \sum_P \Xi_P^2 = 1$ , along with other analogous relations. For a non-stabilizer state, while  $\sum_P \Xi_P = 1$  remains valid,  $1/d^2 \leq \xi < 1$ . A family of SREs,  $\mathcal{M}_\alpha$  are defined by [46]

$$\mathcal{M}_\alpha(|\psi\rangle) = \frac{1}{1-\alpha} \log_2 \sum_P \Xi_P^\alpha - \log_2 d. \quad (2)$$

Out of these measures the stabilizer 2-Rényi entropy  $\mathcal{M}_2(|\psi\rangle)$  has been shown to satisfy property of monotonicity [48, 49]. Here we will pursue  $\mathcal{M}_{\text{lin}}(|\psi\rangle)$ , the linear version of  $\mathcal{M}_2$ ,

$$\mathcal{M}_{\text{lin}}(|\psi\rangle) = 1 - \xi. \quad (3)$$

The main reason behind this choice is that  $\mathcal{M}_{\text{lin}}(|\psi\rangle)$  has been shown to be directly related to some aspect of interplay between entanglement and magic [86], which will become clearer below. Moreover,  $\mathcal{M}_{\text{lin}}(|\psi\rangle)$  has been shown to be a strong monotone [49] and directly yields the stabilizer 2-Rényi entropy through

$$\mathcal{M}_2(|\psi\rangle) = -\log_2 \xi = -\log_2 (1 - \mathcal{M}_{\text{lin}}(|\psi\rangle)). \quad (4)$$

As defined, these measures of magic contain contributions from both local and non-local magic. Given that the local magic can be eliminated, by definition, by applications of local unitary operators, the bi-partite non-local magic <sup>2</sup> is defined by [62, 93]

$$\mathcal{M}_i^{(NL)}(|\psi\rangle) = \min_{\hat{U}_A \otimes \hat{U}_B} \left[ \mathcal{M}_i^{(NL)} \left( \hat{U}_A \otimes \hat{U}_B |\psi\rangle \right) \right], \quad i \equiv \alpha, \text{lin}, \quad (5)$$

where  $A$  and  $B$  denote the two chosen partitions (here the two qubits) and where the minimization is over all possible local unitary transformations on  $A$  and  $B$ , providing a basis-independent quantity. For the two-qubit system, the minimization corresponds to the simple task of searching over the six angles defining transformations over each Bloch sphere. In some instances, this can be accomplished analytically, while in many others it requires a numerical procedure.

It has been recently shown that measures of total magic and non-local magic in a pure state  $|\psi\rangle$  can be related to the anti-flatness of the bi-partite entanglement spectrum of that state. Such anti-flatness is defined by a polynomial function of the reduced density matrix  $\hat{\rho}_A = \text{Tr}_B \hat{\rho}_{AB}$  of subsystem A [86] as

$$\mathcal{F}_A(|\psi\rangle) = \langle \rho_A^2 \rangle - \langle \rho_A \rangle^2 = \text{Tr}(\rho_A^3) - (\text{Tr} \rho_A^2)^2, \quad (6)$$

---

<sup>2</sup> The definition of non-local magic can be straightforwardly generalized to systems with more than two qubits, both for bi-partitions and multi-partitions [62, 93].

and corresponds to the variance of the reduced density matrix. The two contributions to the anti-flatness cancel when the non-zero eigenvalues of  $\hat{\rho}_A$  are equal (flat entanglement spectrum), which occurs if  $|\psi\rangle$  is unentangled or has no magic [86]. It is important to note that, similarly to the non-local magic, the anti-flatness is independent on the local basis, but is not invariant under global Clifford operations.

In Ref. [86] it has been shown that the total linear magic is directly proportional to the average anti-flatness associated with applications of all possible combinations of Clifford gates to the complete state:

$$\langle \mathcal{F}_A(\hat{\Gamma}|\psi)\rangle_{\mathcal{C}} = c(d, d_A) \mathcal{M}_{\text{lin}}(|\psi\rangle), \quad (7)$$

where the left-hand side is the anti-flatness of  $\hat{\Gamma}|\psi\rangle$  averaged over Clifford unitaries  $\hat{\Gamma} \in \mathcal{C}$ , and the proportionality constant  $c(d, d_A)$  is given by

$$c(d, d_A) = \frac{(d^2 - d_A^2)(d_A^2 - 1)}{(d^2 - 1)(d + 2)d_A^2}, \quad (8)$$

where  $d_A$  is the dimensionality of system-A Hilbert space. The averaging over Clifford operators provides a quantity that is Clifford-invariant. At the same time, it re-distributes the magic among local and non-local components, and thus can re-introduce local magic.

Further, Ref. [62] showed that the presence of non-local magic is a necessary and sufficient condition for anti-flatness of the entanglement spectrum<sup>3</sup>, and is lower bounded by the latter. In the present study, we find that the anti-flatness in two-particle scattering (mapped onto two qubits) is exactly proportional to the non-local linear magic.

### III. TWO-PARTICLE SCATTERING

As the dominant force between particles in nuclei and many processes involving fundamental particles, two-particle processes encapsulated by the S-matrix and T-matrix provide the basic building blocks of quantum complexity in many-body systems. For demonstrative purposes, motivated by what might be experimentally possible, we examine the anti-flatness and non-local magic in the spin-sector of low-energy (non-relativistic) S-wave nucleon-nucleon scattering, and high-energy (relativistic) Møller scattering,  $e^-e^- \rightarrow e^-e^-$ . These processes probe different sectors of the fundamental forces of Nature. While the simple frameworks adopted in this work yield similar analytic structures for both processes, they already reveal notable differences in the ability of the underlying forces to generate and remove non-local magic and entanglement.

#### A. Nucleon-Nucleon Scattering

Low-energy  $S$ -wave nucleon-nucleon scattering is described by an S-matrix of the form

$$\hat{S} = \begin{pmatrix} e^{2i\delta_1} & 0 & 0 & 0 \\ 0 & \frac{1}{2}(e^{2i\delta_1} + e^{2i\delta_0}) & \frac{1}{2}(e^{2i\delta_1} - e^{2i\delta_0}) & 0 \\ 0 & \frac{1}{2}(e^{2i\delta_1} - e^{2i\delta_0}) & \frac{1}{2}(e^{2i\delta_1} + e^{2i\delta_0}) & 0 \\ 0 & 0 & 0 & e^{2i\delta_1} \end{pmatrix}, \quad (9)$$

where  $\delta_{0,1}$  are the phase shifts in the  $S = 0$  and  $S = 1$  spin channels. These are the dominant, but not only, channels contributing at low-energies, and a more complete analysis would include contributions from P-wave, SD-mixing (induced by the tensor force) and higher.

When applied to some initial incoming state, the S-matrix in Eq. (9) defines the asymptotic final state of the scattering system. In Ref. [59], we studied the magic power of the scattering S-matrix as the average SRE induced by the S-matrix acting on the set of the 60 two-qubit stabilizer states (listed in App. B):

$$\overline{\mathcal{M}_{\text{lin}}}(\hat{S}) \equiv \frac{1}{60} \sum_{i=1}^{60} \mathcal{M}_{\text{lin}}(\hat{S}|\psi_i). \quad (10)$$

---

<sup>3</sup> The sufficiency condition is verified for most magic measures, except for some particular non-integer SREs [62].

This quantity included both the local and non-local magic powers, which were not separated. In order to separate them, we define here the non-local magic power and anti-flatness power in a similar manner. To further isolate the induced changes of entanglement, we however choose to restrict the average to the 36 tensor-product states (formed from the 6 single-qubit stabilizer states) only. That is,

$$\overline{\mathcal{M}}_{\text{lin}}^{(NL)}(\hat{\mathbf{S}}) \equiv \frac{1}{36} \sum_{i=1}^{36} \mathcal{M}_{\text{lin}}^{(NL)}(\hat{\mathbf{S}}|\psi_i\rangle) , \quad (11)$$

$$\overline{\mathcal{F}}_A(\hat{\mathbf{S}}) \equiv \frac{1}{36} \sum_{i=1}^{36} \mathcal{F}_A(\hat{\mathbf{S}}|\psi_i\rangle) . \quad (12)$$

Quantities averaged over the full set of stabilizer states are denoted with a single bar  $\overline{\mathcal{O}}$ , while those averaged over the tensor-product stabilizer states are denoted with a double bar  $\overline{\overline{\mathcal{O}}}$ .

Direct optimization over the 6 Euler angles defining the two Bloch spheres yields the following expression for the non-local magic power, which we find to be exactly equal to four times the anti-flatness power <sup>4</sup>

$$4 \overline{\overline{\mathcal{F}}}_A(\hat{S}) = \overline{\overline{\mathcal{M}}}_{\text{lin}}^{(NL)}(\hat{S}) = \frac{1}{48} (11 + 5 \cos(4\Delta\delta)) \sin^2(2\Delta\delta) , \quad (13)$$

where  $\Delta\delta = \delta_1 - \delta_0$ . This is to be compared to the total magic power, which is given by [59]

$$\overline{\mathcal{M}}_{\text{lin}}(\hat{S}) = \frac{3}{20} (3 + \cos(4\Delta\delta)) \sin^2(2\Delta\delta) . \quad (14)$$

The results obtained using Nijmegen Nijm93 phase shifts [94, 95] (determined from fitting NN experimental data) are shown in Fig. 1. For comparison, we also show the linear magic power  $\overline{\overline{\mathcal{M}}}_{\text{lin}}(\hat{S})$  averaged over tensor-product stabilizer states only, along with the entanglement power for information <sup>5</sup>. It is seen that in the regime  $p_{\text{lab}} \lesssim 150$  MeV, only

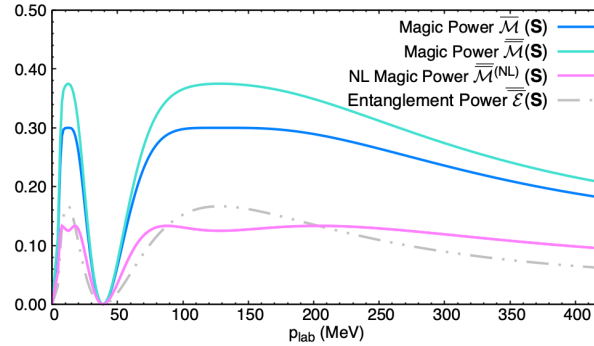


FIG. 1. The non-local magic power,  $\overline{\overline{\mathcal{M}}}_{\text{lin}}^{(NL)}(\hat{S})$  and the total magic powers  $\overline{\mathcal{M}}_{\text{lin}}(\hat{S})$  and  $\overline{\overline{\mathcal{M}}}_{\text{lin}}(\hat{S})$  for low-energy S-wave nucleon-nucleon scattering as a function of momentum in the laboratory. The difference in phase shifts are determined from the Nijmegen phase-shift analysis [94, 95]. The entanglement power is also shown, as a dashed line.

about one third of the magic generated is non-local, while the rest can be eliminated via local basis transformation. We have also numerically verified the relation in Eq. (7),  $\langle \mathcal{F}_A(\Gamma|\psi) \rangle_C = c(d, d_A) \mathcal{M}_{\text{lin}}(|\psi\rangle)$ .

We analyze in more detail the individual contribution of outgoing states produced from different groups of initial stabilizer states. As we identified previously [59], these 36 states divide into 3 groups, Group-1, 2, 3, in which there are 6, 6, 24 tensor-product initial states, respectively. These groups are chosen so that the states in each group yield the same total outgoing magic, and are listed in App. C. The anti-flatness is again equal to four times the non-local

<sup>4</sup> We empirically find that this is verified for any two-qubit state  $|\psi\rangle$ , *i.e.*  $4 \mathcal{F}_A(|\psi\rangle) = \mathcal{M}_{\text{lin}}^{(NL)}(|\psi\rangle)$ .

<sup>5</sup> The corresponding entanglement power is given by [3, 59]

$$\overline{\overline{\mathcal{E}}}(\hat{S}) = \frac{1}{6} \sin^2(2\Delta\delta) . \quad (15)$$

linear magic, and interestingly, we find that, in each group, the non-local linear magic is also proportional to the total linear magic:

$$\text{Group - 1 : } \mathcal{F}_A = \mathcal{M}_{\text{lin}}^{(NL)} = \mathcal{M}_{\text{lin}} = 0 , \quad (16)$$

$$\text{Group - 2 : } 4 \mathcal{F}_A = \mathcal{M}_{\text{lin}}^{(NL)} = \mathcal{M}_{\text{lin}} = \frac{1}{4} \sin^2(4\Delta\delta) , \quad (17)$$

$$\text{Group - 3 : } 4 \mathcal{F}_A = \mathcal{M}_{\text{lin}}^{(NL)} = \frac{1}{3} \mathcal{M}_{\text{lin}} = \frac{1}{32} (7 + \cos(4\Delta\delta)) \sin^2(2\Delta\delta) . \quad (18)$$

The proportionality constant is however different for each of the groups. In contrast to Groups-2,3, scattering of Group-1 states does not create magic or anti-flatness. For scattering of states in Group-2, the total magic of the final states is saturated by the non-local magic. That is to say that all the magic generated is bound to the outgoing system and there is no magic in the final state that can be removed by changes of local basis. In Group-3, the non-local magic constitutes only a third of the total magic. In App. C, we show the magic, non-local magic (here equivalent to anti-flatness) and entanglement for scattering of states in each group, and also show results when considering entangled stabilizer states.

Tensor-product stabilizer states representative of each group, denoted by  $|\psi_{1,2,3}\rangle$ , that are candidates for experimental initial-state preparation are,

$$|\psi_1\rangle = |\uparrow\rangle \otimes |\uparrow\rangle , \quad |\psi_2\rangle = |\uparrow\rangle \otimes |\downarrow\rangle , \quad |\psi_3\rangle = \frac{1}{\sqrt{2}} [ |\uparrow\rangle + |\downarrow\rangle ] \otimes |\uparrow\rangle , \quad (19)$$

corresponding to states 33, 34 and 25 in Table. I. Experimentally, the wavefunction associated with the selected Group-3 state can be prepared by a single-spin  $\pi/2$  rotation about the y-axis.

We have previously found that the entanglement and (total) magic power in  $\Sigma^-n$  scattering is large and energy independent over a large range, after a rapid rise at low-energies [59]. Extending the above analysis to the  $\Sigma^-n$  sector, shows that the non-local magic (or anti-flatness) exhibit similar behaviors. They rise rapidly and remain constant, with a small amplitude modulation over an extended energy interval. Non-local magic is found to capture less than half ( $\simeq 0.4$ ) of the total magic, and this fraction remains constant even at large momenta.

## B. High-Energy Møller Scattering

High-energy Møller scattering provides a sensitive probe for new physics, and establishes increasingly precise constraints on electroweak interactions in the Standard Model. For example, the MOLLER experiment at the Thomas Jefferson National Accelerator Facility [96, 97] is designed to measure the parity-violating asymmetry,  $A_{PV}$ , to a precision of 0.7 ppb, thereby probing the interference of amplitude from the exchange of a neutral weak-gauge boson,  $Z^0$ , and the electromagnetic amplitude with remarkable sensitivity. This process also provides somewhat of a complementary process to NN scattering for exposing non-local magic and anti-flatness in two-body scattering. It has been considered in previous works exploring quantum complexity in fundamental processes, including (the first) work that highlighted that entanglement seems to be maximal [1, 2], and a recent consideration of total magic [56]. Following Ref. [56], instead of considering the structure of the complete S-matrix, we consider the final state wavefunction generated at leading order in perturbation theory (in the electromagnetic coupling constant,  $e$ ) by a single insertion of the T-matrix. This preserves unitarity up to  $\mathcal{O}(e^4)$ , and necessarily requires a projective measurement on the two-electron final state.

The post-scattering wavefunction can be determined from the expressions in App. D, and using the helicity-amplitude basis, the scattering amplitude matrix in the high-energy limit ( $m_e \rightarrow 0$ ) becomes [1, 2, 98],

$$\mathcal{A} \propto \begin{pmatrix} -8 \csc^2(\theta) & 0 & 0 & 0 \\ 0 & -2 \cot^2\left(\frac{\theta}{2}\right) & 2 \tan^2\left(\frac{\theta}{2}\right) & 0 \\ 0 & 2 \tan^2\left(\frac{\theta}{2}\right) & -2 \cot^2\left(\frac{\theta}{2}\right) & 0 \\ 0 & 0 & 0 & -8 \csc^2(\theta) \end{pmatrix} , \quad (20)$$

where  $\theta$  is the center-of-momentum scattering angle. The proportionality constant, including factors of  $e^2$  are inconsequential upon renormalizing the final state wavefunction. For any initial state wavefunction,  $|\psi\rangle$ , the final state wavefunction is given by  $|\chi\rangle = \mathcal{N} \mathcal{A}|\psi\rangle$ . The normalization constant,  $\mathcal{N}$ , is determined (up to an overall phase) by  $\langle\chi|\chi\rangle = 1$ . In contrast to Ref. [56] with amplitudes given in terms of the computational basis (because of the basis

dependence of the total magic), we use the helicity basis to write  $\mathcal{A}$ , but any single-particle basis would have served our purposes. The total magic, non-local magic and anti-flatness powers take the same expression as in Eqs. (10), (11) and (12), with  $\hat{S}|\psi_i\rangle \rightarrow \mathcal{N}\hat{\mathcal{A}}|\psi_i\rangle$ .

There are five different groups of stabilizer states with respect to the total magic injected by the scattering amplitude in Eq. (20), which are given in Eq. (D7) in App. D. Each state in a given group gives rise to a final state with the same total magic. Representative initial tensor-product states from each group are

$$\begin{aligned} |\psi_1\rangle &= |\uparrow\rangle \otimes |\uparrow\rangle, \quad |\psi_2\rangle = \frac{1}{\sqrt{2}}[|\uparrow\rangle + |\downarrow\rangle] \otimes \frac{1}{\sqrt{2}}[|\uparrow\rangle + |\downarrow\rangle], \quad |\psi_3\rangle = \frac{1}{\sqrt{2}}[|\uparrow\rangle + |\downarrow\rangle] \otimes \frac{1}{\sqrt{2}}[|\uparrow\rangle - |\downarrow\rangle], \\ |\psi_4\rangle &= |\uparrow\rangle \otimes |\downarrow\rangle, \quad |\psi_{5a}\rangle = \frac{1}{\sqrt{2}}[|\uparrow\rangle + i|\downarrow\rangle] \otimes \frac{1}{\sqrt{2}}[|\uparrow\rangle + |\downarrow\rangle], \quad |\psi_{5b}\rangle = |\uparrow\rangle \otimes \frac{1}{\sqrt{2}}[|\uparrow\rangle + |\downarrow\rangle]. \end{aligned} \quad (21)$$

The values of the total linear magic,  $\mathcal{M}_{\text{lin}}(|\chi_i\rangle)$ , defined in Eq. (3), of the associated wavefunction  $|\chi_i\rangle = \mathcal{N}\hat{\mathcal{A}}|\psi_i\rangle$  for each of the groups, are

$$\begin{aligned} \text{Group - 1} : \mathcal{M}_{\text{lin}} &= 0, \\ \text{Group - 2} : \mathcal{M}_{\text{lin}} &= \frac{64 \sin^4(\theta) \cos^2(\theta)}{(\cos(2\theta) + 3)^4}, \\ \text{Group - 3} : \mathcal{M}_{\text{lin}} &= \frac{1024 \sin^4(\theta)(20 \cos(2\theta) + \cos(4\theta) + 43)^2}{(12 \cos(2\theta) + \cos(4\theta) + 51)^4}, \\ \text{Group - 4} : \mathcal{M}_{\text{lin}} &= \frac{4 \cot^8\left(\frac{\theta}{2}\right) (\cot^8\left(\frac{\theta}{2}\right) - 1)^2}{(\cot^8\left(\frac{\theta}{2}\right) + 1)^4}, \\ \text{Group - 5} : \mathcal{M}_{\text{lin}} &= \frac{32 \sin^4(\theta)(799 \cos(2\theta) - 10 \cos(4\theta) + \cos(6\theta) + 1258)}{(\cos(2\theta) + 7)^6}. \end{aligned} \quad (22)$$

The corresponding anti-flatness is found to recover the results of numerical minimization of  $\mathcal{M}_{\text{lin}}^{(NL)}$  for each group, which are found to be

$$\begin{aligned} \text{Group - 1} : \mathcal{M}_{\text{lin}}^{(NL)} &= 4 \mathcal{F}_A = \mathcal{M}_{\text{lin}} = 0, \\ \text{Group - 2} : \mathcal{M}_{\text{lin}}^{(NL)} &= 4 \mathcal{F}_A = \mathcal{M}_{\text{lin}}, \\ \text{Group - 3} : \mathcal{M}_{\text{lin}}^{(NL)} &= 4 \mathcal{F}_A = \mathcal{M}_{\text{lin}}, \\ \text{Group - 4} : \mathcal{M}_{\text{lin}}^{(NL)} &= 4 \mathcal{F}_A = \mathcal{M}_{\text{lin}}, \\ \text{Group - 5a} : \mathcal{M}_{\text{lin}}^{(NL)} &= 4 \mathcal{F}_A = \frac{256 \sin^4(\theta)(\cos(2\theta) + 15)^2(28 \cos(2\theta) + \cos(4\theta) + 35)}{(\cos(2\theta) + 7)^8} \leq \mathcal{M}_{\text{lin}}, \\ \text{Group - 5b} : \mathcal{M}_{\text{lin}}^{(NL)} &= 4 \mathcal{F}_A = \frac{128 \sin^8(\theta)(175 \cos(2\theta) + 18 \cos(4\theta) + \cos(6\theta) + 318)}{(\cos(2\theta) + 7)^8} \ll \mathcal{M}_{\text{lin}}. \end{aligned} \quad (23)$$

Notice that the states in Group-5 produce final states that have two different values of anti-flatness. Therefore, we further sub-divide these states into Group-5a and Group-5b, as given in Eq. (D8) in App. D. For all states, the relation  $\mathcal{M}_{\text{lin}}^{(NL)}(|\chi_i\rangle) = 4 \mathcal{F}_A(|\chi_i\rangle)$  is verified. For Group-1,2,3,4, the outgoing states only exhibit non-local magic as  $\mathcal{M}_{\text{lin}}^{(NL)}(|\chi_i\rangle) = \mathcal{M}_{\text{lin}}(|\chi_i\rangle)$ . This is not the case for outgoing states generated from stabilizer states from Group-5a and Group-5b, which also display some local magic. In finding the non-local magic, we are unable to arrive at closed-form results for  $\mathcal{M}_{\text{lin}}^{(NL)}$  by analytic minimization of local unitary transformations for some of the groups. However, numerical minimization over the two Bloch spheres is found to be effective. The resulting non-local magic, as well as the total magic and anti-flatness, for initial tensor product states in each of the groups, are shown in Fig. 2. For completeness, the total linear magic  $\mathcal{M}_{\text{lin}}(|\chi_i\rangle)$ , linear entanglement entropy, and non-local magic  $\mathcal{M}_{\text{lin}}^{(NL)}(|\chi_i\rangle)$  of the outgoing states  $|\chi_i\rangle = \mathcal{N}|\psi_i\rangle$  for each groups, including for entangled initial states, are shown in Fig. 6 in App. D.

The relation between the anti-flatness averaged over the Clifford group, given in Eq. (7) has been numerically verified. Figure 3 shows the Clifford-averaged anti-flatness and the total linear magic divided by 10 for the states in Group-5a and 5b. The averaged results are consistent with the relation  $\langle \mathcal{F}_A(\Gamma|\psi) \rangle_{\mathcal{C}} = c(d, d_A) \mathcal{M}_{\text{lin}}(|\psi\rangle)$  in Eq. (7), where  $c(d, d_A)$  in Eq. (8) is  $c(4, 2) = 1/10$ . The estimators of  $\langle \mathcal{F}_A(\Gamma|\psi) \rangle_{\mathcal{C}}$  in Fig. 3 at each angle were determined

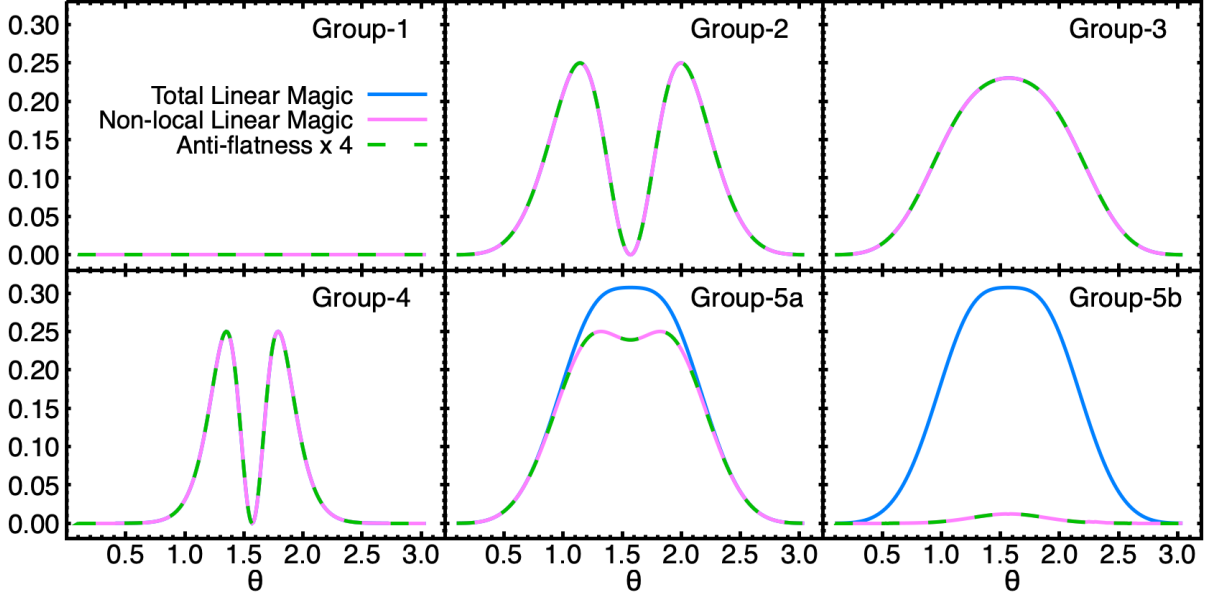


FIG. 2. The linear magic,  $\mathcal{M}_{\text{lin}}(|\chi_i\rangle)$ , the non-local linear magic,  $\mathcal{M}_{\text{lin}}^{(NL)}(|\chi_i\rangle)$  and the anti-flatness,  $\mathcal{F}_A(|\chi_i\rangle)$  (multiplied by a factor 4), for outgoing states  $|\chi_i\rangle = \mathcal{N}\hat{A}|\psi_i\rangle$ , corresponding to the distinct groups of initial-state helicity wavefunctions  $|\psi_i\rangle$  for high-energy Møller scattering. The upper panels from left to right show the results for tensor-product states from Group-1, 2, 3, while the lower panels show the results for Group-4, 5a, 5b. The green curves associated with the  $\mathcal{M}_{\text{lin}}$  are from Eq. (22), while the dashed blue curves associated with the  $\mathcal{F}_A$  are from Eq. (23). The pink curves are from numerical minimization of  $\mathcal{M}_{\text{lin}}^{(NL)}(|\chi_i\rangle)$ , using Eq. (5).

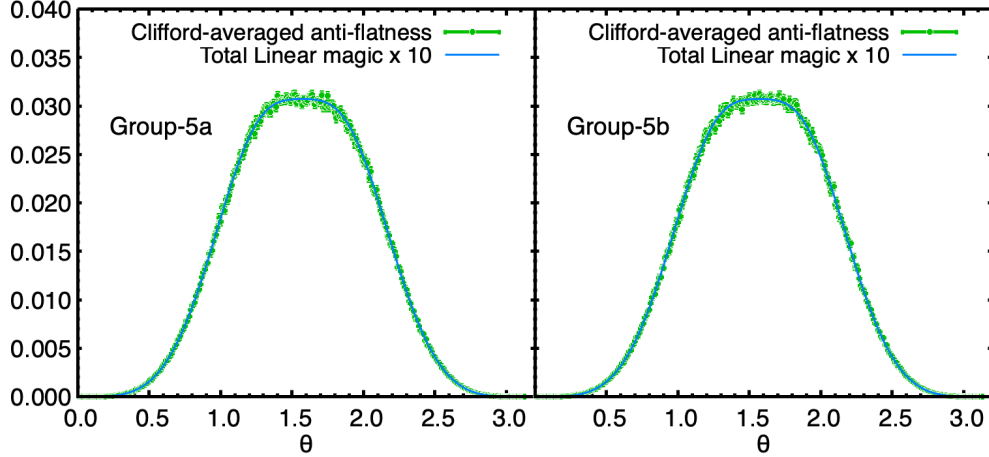


FIG. 3. The Clifford-averaged anti-flatness,  $\langle \mathcal{F}_A(\Gamma|\chi_i) \rangle_C$ , (green points) compared with  $c(d, d_A)\mathcal{M}_{\text{lin}}(|\chi_i\rangle)$  (blue curve) in Møller scattering from initial states  $|\psi_{5a}\rangle$  (left panel) and  $|\psi_{5b}\rangle$  (right panel) in Eq. (21). The un-averaged values of anti-flatness are shown in Fig. 2.

from the mean and standard deviation of an ensemble of  $\mathcal{F}_A$  generated from  $5 \times 10^3$  samples of random Clifford gates applied to the final state wavefunction.

The current Møller scattering experiment (MOLLER) at JLab [96, 97] is able to prepare arbitrary polarized initial states with high precision, but currently lacks the capability to measure spin components of final state particles. This means that the anti-flatness cannot be measured with this generation of experiment. However, with sufficient motivation, there could be potential for including such capabilities in a next-generation MOLLER program.

### C. Non-local Magic Generation from Entangled Initial States: Nuclear Force Versus Quantum Electrodynamics

We have so far focused on the non-local magic and anti-flatness produced in scattering processes in which the two particles are initially unentangled. Since non-local magic requires entanglement, this allowed us to isolate the effectiveness of the underlying interaction to generate both the needed entanglement and the corresponding non-local magic. This is also justified from an experimental point of view, as in laboratory scattering experiments the initial incoming particles are typically unentangled.

Nevertheless it is also interesting to investigate the effect of scattering when the two initial particles are prepared in an entangled stabilizer state. These states are those numbered 37 to 60 in Table I in App. B. They are maximally entangled but possess, by definition, no magic (local or non-local) and no anti-flatness. Thus studying scattering from these states can tell us about whether the underlying interaction can build on the initial entanglement to generate anti-flatness (complex entanglement patterns), and non-local magic. For example, is the non-local magic enhanced when the initial states are entangled?

Figure 4 shows the final-state total magic, non-local magic (or anti-flatness) and linear entanglement entropy averaged over initial entangled stabilizer states for both NN and Møller scattering.<sup>6</sup> While magic is produced in both

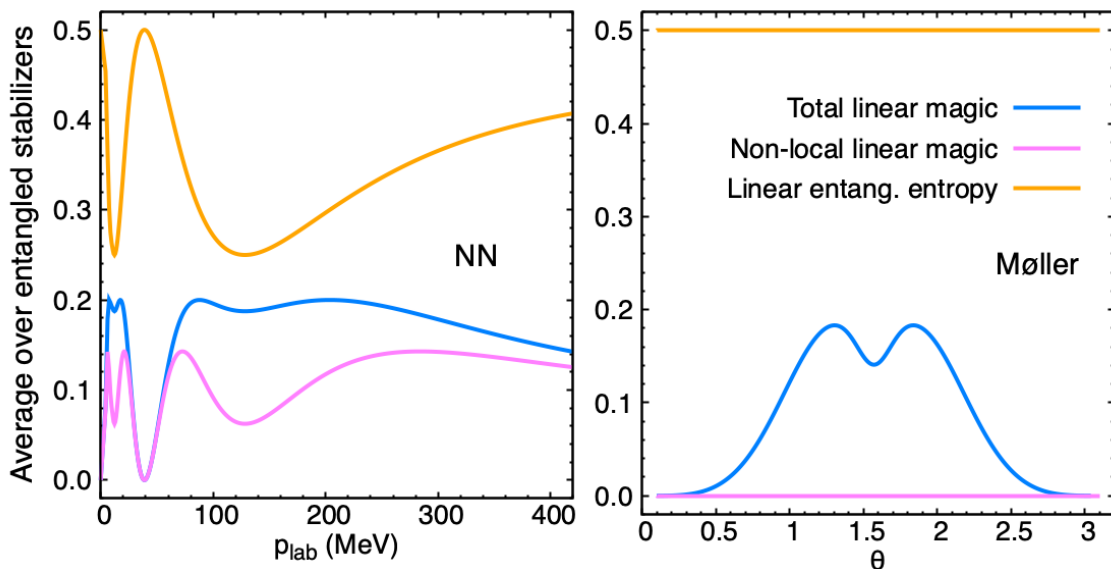


FIG. 4. The total linear magic, non-local linear magic (anti-flatness), and linear entanglement entropy in NN scattering and Møller scattering final states, averaged over all 24 entangled stabilizer states.

processes, Møller scattering does not generate non-local magic when the initial stabilizer states are entangled, and the outgoing particles remain maximally entangled. This means that the outgoing states are themselves stabilizer states in a different local basis. We also observe the same effect in other quantum electrodynamics processes such as  $e^+e^- \rightarrow \mu^+\mu^-$ . More generally, for arbitrary 2-qubit initial states, the ability of the interaction to disentangle during those processes is very small, when compared to the entangling power. In contrast, the nuclear force in low-energy S-wave NN scattering disentangles maximally entangled particles, and produces non-local magic (or anti-flatness). In fact it is shown in Fig. 5 of App. C that the “dis-entangling power” is about the same or larger than the entangling power in this process, depending on the group of initial states. We also find that the non-local magic produced from entangled and unentangled states within group-1 and within group-2 is the same, while initial entanglement in states from Group-3 yield greater non-local magic, with a different structure.

<sup>6</sup> The difference between the average final-state linear entanglement entropy and its maximal value of 1/2 can be identified as the “dis-entanglement” power, which is seen to be zero in the Møller scattering process.

#### IV. SUMMARY

Towards a better understanding of the generation of quantum complexity in few-body and many-body systems from fundamental interactions, we have considered the non-local magic and anti-flatness in two-particle scattering processes. While large-scale non-local magic and anti-flatness in a physical system drive the need for quantum computers in simulations, in two-particle processes they define beyond-classical, basis-independent quantum observables and are fundamental elements of larger systems. We have focused on the spin-space structure of two such processes, low-energy S-wave nucleon-nucleon scattering and high-energy Møller scattering. Starting with each of the tensor-product two-qubit stabilizer states, we have shown that there are a small number of groups of final-states exhibiting the same magic, and whose non-linear magic and anti-flatness are related by a factor of four. From an experimental standpoint, this relationship is convenient because only the spin of one of the final-state particles is required to be measured from polarized initial states, and not the spin correlations of both particles, as would be required for a CHSH measurement. We have also found substantial differences in the effectiveness of quantum electrodynamics and nuclear forces to disentangle and induce non-local magic in the scattering processes, when the initial particles are maximally entangled.

One may, once again, speculate about the connections between symmetries and the minimal entangling power of the S-matrix in confining theories. In Ref. [3], the vanishing entangling power resulting from identical phase shifts (or phase shifts different by  $\pi/2$ ) was connected to enhanced emergent spin-flavor symmetries in nucleon-nucleon scattering (Wigner's SU(4) symmetry) and in hyperon-nucleon scattering (SU(16) symmetry). The latter is a larger group than the SU(6) symmetry group required by the large- $N_c$  limit of QCD, while Wigner's symmetry is the same. Given the results presented in this work, it is not possible to separate vanishing entanglement power from vanishing non-local magic power. Given that some of the large-scale entangled states can be prepared efficiently with classical resources, while those with large-scale non-local magic cannot, we highlight the fact that minimizing fluctuations in entanglement also minimize fluctuations in non-local magic.

#### ACKNOWLEDGMENTS

We would like to thank Krishna Kumar for enlightening discussions about MOLLER and other electron scattering experiments. We are grateful to the organizers and participants of the First <sup>7</sup> and Second <sup>8</sup> International Workshops on Many-Body Quantum Magic. This work was supported, in part, by Universität Bielefeld (Caroline), and by U.S. Department of Energy, Office of Science, Office of Nuclear Physics, InQubator for Quantum Simulation (IQUS)<sup>9</sup> under Award Number DOE (NP) Award DE-SC0020970 via the program on Quantum Horizons: QIS Research and Innovation for Nuclear Science<sup>10</sup> (Martin). This work was also supported, in part, through the Department of Physics<sup>11</sup> and the College of Arts and Sciences<sup>12</sup> at the University of Washington. We have made extensive use of Wolfram Mathematica [99].

- 
- [1] A. Cervera-Lierta, J. I. Latorre, J. Rojo, and L. Rottoli, Maximal Entanglement in High Energy Physics, *SciPost Phys.* **3**, 036 (2017).
  - [2] A. Cervera-Lierta, *Maximal entanglement: Applications in quantum information and particle physics* (2019), arXiv:1906.12099 [quant-ph].
  - [3] S. R. Beane, D. B. Kaplan, N. Klco, and M. J. Savage, Entanglement Suppression and Emergent Symmetries of Strong Interactions, *Phys. Rev. Lett.* **122**, 102001 (2019), arXiv:1812.03138 [nucl-th].
  - [4] I. Low and T. Mehen, Symmetry from entanglement suppression, *Phys. Rev. D* **104**, 074014 (2021), arXiv:2104.10835 [hep-th].
  - [5] S. R. Beane, R. C. Farrell, and M. Varma, Entanglement minimization in hadronic scattering with pions, *International Journal of Modern Physics A* **36**, 10.1142/s0217751x21502055 (2021).
  - [6] Q. Liu, I. Low, and T. Mehen, Minimal entanglement and emergent symmetries in low-energy qcd, *Physical Review C* **107**, 10.1103/physrevc.107.025204 (2023).
  - [7] Q. Liu and I. Low, Hints of entanglement suppression in hyperon-nucleon scattering, *Physics Letters B* **856**, 138899 (2024).

<sup>7</sup> <https://mbqm.tii.ae/>

<sup>8</sup> <https://iqus.uw.edu/events/iqus-workshop-2025-2/>

<sup>9</sup> <https://iqus.uw.edu>

<sup>10</sup> <https://science.osti.gov/np/Research/Quantum-Information-Science>

<sup>11</sup> <https://phys.washington.edu>

<sup>12</sup> <https://www.artsci.washington.edu>

- [8] D. B. Kaplan and M. J. Savage, The spin-flavor dependence of nuclear forces from large- $n$  qcd, *Physics Letters B* **365**, 244–251 (1996).
- [9] N. McGinnis, *Symmetry, entanglement, and the  $s$ -matrix* (2025), [arXiv:2504.21079 \[hep-th\]](#).
- [10] [NPLQCD], M. L. Wagman, F. Winter, E. Chang, Z. Davoudi, W. Detmold, K. Orginos, M. J. Savage, and P. E. Shanahan, Baryon-Baryon Interactions and Spin-Flavor Symmetry from Lattice Quantum Chromodynamics, *Phys. Rev. D* **96**, 114510 (2017), [arXiv:1706.06550 \[hep-lat\]](#).
- [11] M. Carena, I. Low, C. E. M. Wagner, and M.-L. Xiao, *Entanglement suppression, enhanced symmetry and a standard-model-like higgs boson* (2023), [arXiv:2307.08112 \[hep-ph\]](#).
- [12] G. Busoni, J. Gargalionis, E. N. Wallace, and M. J. White, Emergent symmetry in a two-higgs-doublet model from quantum information and nonstabilizerness, *Physical Review D* **112**, 10.1103/r5ps-pmh3 (2025).
- [13] S. Chang and G. Jacobo, Consequences of minimal entanglement in bosonic field theories, *Physical Review D* **110**, 10.1103/physrevd.110.096020 (2024).
- [14] T.-R. Hu, K. Sone, F.-K. Guo, T. Hyodo, and I. Low, *Entanglement suppression, quantum statistics and symmetries in spin-3/2 baryon scatterings* (2025), [arXiv:2506.08960 \[hep-ph\]](#).
- [15] C. Nunez, A. Cervera-Lierta, and J. I. Latorre, *Universality of entanglement in gluon dynamics* (2025), [arXiv:2504.15353 \[hep-th\]](#).
- [16] D. Bai and Z. Ren, Entanglement generation in few-nucleon scattering, *Phys. Rev. C* **106**, 064005 (2022), [arXiv:2212.11092 \[nucl-th\]](#).
- [17] D. Bai, Toward experimental determination of spin entanglement of nucleon pairs, *Phys. Rev. C* **109**, 034001 (2024), [arXiv:2308.12327 \[nucl-th\]](#).
- [18] D. Bai, Spin entanglement in neutron-proton scattering, *Phys. Lett. B* **845**, 138162 (2023), [arXiv:2306.04918 \[nucl-th\]](#).
- [19] G. A. Miller, Entanglement maximization in low-energy neutron-proton scattering, *Phys. Rev. C* **108**, L031002 (2023), [arXiv:2306.03239 \[nucl-th\]](#).
- [20] G. A. Miller, Entanglement of elastic and inelastic scattering, *Phys. Rev. C* **108**, L041601 (2023), [arXiv:2306.14800 \[nucl-th\]](#).
- [21] T. Kirchner, W. El-Kamhawy, and H.-W. Hammer, Entanglement in Few-Nucleon Scattering Events, *Few Body Syst.* **65**, 29 (2024), [arXiv:2312.14484 \[nucl-th\]](#).
- [22] D. Bai and Z. Ren, Spin entanglement of multinucleons: experimental prospects, (2024), [arXiv:2404.09116 \[nucl-th\]](#).
- [23] A. L. Cavallin, O. Thim, and C. Forssén, Entanglement and accidental symmetries in the nucleon-nucleon system, (2025), [arXiv:2510.09466 \[nucl-th\]](#).
- [24] C. W. Johnson and O. C. Gorton, Proton-neutron entanglement in the nuclear shell model, *J. Phys. G* **50**, 045110 (2023), [arXiv:2210.14338 \[nucl-th\]](#).
- [25] O. Legeza, L. Veis, A. Poves, and J. Dukelsky, Advanced density matrix renormalization group method for nuclear structure calculations, *Phys. Rev. C* **92**, 051303 (2015).
- [26] A. T. Kruppa, J. Kovács, P. Salamon, and O. Legeza, Entanglement and correlation in two-nucleon systems, *J. Phys. G* **48**, 025107 (2021), [arXiv:2006.07448 \[nucl-th\]](#).
- [27] C. Robin, M. J. Savage, and N. Pillet, Entanglement Rearrangement in Self-Consistent Nuclear Structure Calculations, *Phys. Rev. C* **103**, 034325 (2021), [arXiv:2007.09157 \[nucl-th\]](#).
- [28] A. T. Kruppa, J. Kovács, P. Salamon, O. Legeza, and G. Zaránd, Entanglement and seniority, *Phys. Rev. C* **106**, 024303 (2022), [arXiv:2112.15513 \[nucl-th\]](#).
- [29] E. Pazy, Entanglement entropy between short range correlations and the Fermi sea in nuclear structure, *Phys. Rev. C* **107**, 054308 (2023), [arXiv:2206.10702 \[nucl-th\]](#).
- [30] A. Tichai, S. Knecht, A. T. Kruppa, O. Legeza, C. P. Moca, A. Schwenk, M. A. Werner, and G. Zarand, Combining the in-medium similarity renormalization group with the density matrix renormalization group: Shell structure and information entropy, *Phys. Lett. B* **845**, 138139 (2023), [arXiv:2207.01438 \[nucl-th\]](#).
- [31] A. Pérez-Obiol, S. Masot-Llima, A. M. Romero, J. Menéndez, A. Rios, A. García-Sáez, and B. Juliá-Díaz, Quantum entanglement patterns in the structure of atomic nuclei within the nuclear shell model, *Eur. Phys. J. A* **59**, 240 (2023), [arXiv:2307.05197 \[nucl-th\]](#).
- [32] C. Gu, Z. H. Sun, G. Hagen, and T. Papenbrock, Entanglement entropy of nuclear systems, *Phys. Rev. C* **108**, 054309 (2023), [arXiv:2303.04799 \[nucl-th\]](#).
- [33] Q. Liu and I. Low, Hints of entanglement suppression in hyperon-nucleon scattering (2023), [arXiv:2312.02289 \[hep-ph\]](#).
- [34] A. Bulgac, M. Kafker, and I. Abdurrahman, Measures of complexity and entanglement in many-fermion systems, *Phys. Rev. C* **107**, 044318 (2023), [arXiv:2203.04843 \[nucl-th\]](#).
- [35] A. Bulgac, Entanglement entropy, single-particle occupation probabilities, and short-range correlations, *Phys. Rev. C* **107**, L061602 (2023), [arXiv:2203.12079 \[nucl-th\]](#).
- [36] J. Faba, V. Martín, and L. Robledo, Two-orbital quantum discord in fermion systems, *Phys. Rev. A* **103**, 032426 (2021).
- [37] J. Faba, V. Martín, and L. Robledo, Correlation energy and quantum correlations in a solvable model, *Phys. Rev. A* **104**, 032428 (2021), [arXiv:2106.15993 \[quant-ph\]](#).
- [38] J. Faba, V. Martín, and L. Robledo, Analysis of quantum correlations within the ground state of a three-level Lipkin model, *Phys. Rev. A* **105**, 062449 (2022), [arXiv:2203.09400 \[quant-ph\]](#).
- [39] S. M. Hengstenberg, C. E. P. Robin, and M. J. Savage, Multi-body entanglement and information rearrangement in nuclear many-body systems: a study of the Lipkin–Meshkov–Glick model, *Eur. Phys. J. A* **59**, 231 (2023), [arXiv:2306.16535 \[nucl-th\]](#).
- [40] D. Lacroix, Entanglement in selected Binary Tree States: Dicke/Total spin states, particle number projected BCS states,

- (2024), [arXiv:2405.03647 \[nucl-th\]](#).
- [41] F. Bröckemeier, S. M. Hengstenberg, J. W. T. Keeble, C. E. P. Robin, F. Rocco, and M. J. Savage, Quantum magic and multipartite entanglement in the structure of nuclei, *Phys. Rev. C* **111**, 034317 (2025), [arXiv:2409.12064 \[nucl-th\]](#).
  - [42] D. Gottesman, [The heisenberg representation of quantum computers](#) (1998), [arXiv:quant-ph/9807006 \[quant-ph\]](#).
  - [43] S. Aaronson and D. Gottesman, Improved simulation of stabilizer circuits, *Physical Review A* **70**, 10.1103/physreva.70.052328 (2004).
  - [44] S. Bravyi and D. Gosset, Improved classical simulation of quantum circuits dominated by clifford gates, *Physical Review Letters* **116**, 10.1103/physrevlett.116.250501 (2016).
  - [45] S. Bravyi and A. Kitaev, Universal quantum computation with ideal Clifford gates and noisy ancillas, *Phys. Rev. A* **71**, 022316 (2005), [arXiv:quant-ph/0403025](#).
  - [46] L. Leone, S. F. E. Oliviero, and A. Hama, Stabilizer Rényi Entropy, *Phys. Rev. Lett.* **128**, 050402 (2022), [arXiv:2106.12587 \[quant-ph\]](#).
  - [47] T. Haug and L. Piroli, Quantifying nonstabilizerness of matrix product states, *Phys. Rev. B* **107**, 035148 (2023), [arXiv:2207.13076 \[quant-ph\]](#).
  - [48] T. Haug and L. Piroli, Stabilizer entropies and nonstabilizerness monotones, *Quantum* **7**, 1092 (2023), [arXiv:2303.10152 \[quant-ph\]](#).
  - [49] L. Leone and L. Bittel, Stabilizer entropies are monotones for magic-state resource theory, (2024), [arXiv:2404.11652 \[quant-ph\]](#).
  - [50] L. Bittel and L. Leone, Operational interpretation of the Stabilizer Entropy, (2025), [arXiv:2507.22883 \[quant-ph\]](#).
  - [51] I. Chernyshev, C. E. P. Robin, and M. J. Savage, Quantum magic and computational complexity in the neutrino sector, *Phys. Rev. Res.* **7**, 023228 (2025), [arXiv:2411.04203 \[quant-ph\]](#).
  - [52] L. Ebner, B. Müller, A. Schäfer, L. Schmotzer, C. Seidl, and X. Yao, Entanglement properties of su(2) gauge theory, *Communications Physics* **8**, 10.1038/s42005-025-02298-5 (2025).
  - [53] P. R. N. Falcão, P. S. Tarabunga, M. Frau, E. Tirrito, J. Zakrzewski, and M. Dalmonte, Nonstabilizerness in u(1) lattice gauge theory, *Phys. Rev. B* **111**, L081102 (2025).
  - [54] C. D. White and M. J. White, Magic states of top quarks, *Phys. Rev. D* **110**, 116016 (2024).
  - [55] Observation of magic states of top quark pairs produced in proton-proton collisions at  $\sqrt{s} = 13$  TeV, (2025).
  - [56] Q. Liu, I. Low, and Z. Yin, Quantum Magic in Quantum Electrodynamics, (2025), [arXiv:2503.03098 \[quant-ph\]](#).
  - [57] Q. Liu, I. Low, and Z. Yin, A Quantum Computational Determination of the Weak Mixing Angle in the Standard Model, (2025), [arXiv:2509.18251 \[hep-ph\]](#).
  - [58] J. Gargalionis, N. Moynihan, S. Trifinopoulos, E. N. V. Wallace, C. D. White, and M. J. White, Spin versus Magic: Lessons from Gluon and Graviton Scattering, (2025), [arXiv:2508.14967 \[hep-th\]](#).
  - [59] C. E. P. Robin and M. J. Savage, The Magic in Nuclear and Hypernuclear Forces, (2024), [arXiv:2405.10268 \[nucl-th\]](#).
  - [60] C. E. P. Robin, Stabilizer-Accelerated Quantum Many-Body Ground-State Estimation, (2025), [arXiv:2505.02923 \[quant-ph\]](#).
  - [61] M. Beverland, E. Campbell, M. Howard, and V. Kliuchnikov, Lower bounds on the non-Clifford resources for quantum computations, *Quantum Sci. Technol.* **5**, 035009 (2020), [arXiv:1904.01124 \[quant-ph\]](#).
  - [62] C. Cao, G. Cheng, A. Hama, L. Leone, W. Munizzi, and S. F. E. Oliviero, Gravitational back-reaction is magical, (2024), [arXiv:2403.07056 \[hep-th\]](#).
  - [63] D. Iannotti, G. Esposito, L. C. Venuti, and A. Hama, Entanglement and Stabilizer entropies of random bipartite pure quantum states, *Quantum* **9**, 1797 (2025), [arXiv:2501.19261 \[quant-ph\]](#).
  - [64] S. Bravyi, D. Browne, P. Calpin, E. Campbell, D. Gosset, and M. Howard, Simulation of quantum circuits by low-rank stabilizer decompositions, *Quantum* **3**, 181 (2019).
  - [65] S. Bravyi, G. Smith, and J. A. Smolin, Trading classical and quantum computational resources, *Phys. Rev. X* **6**, 021043 (2016).
  - [66] S. Bravyi and A. Kitaev, Universal quantum computation with ideal clifford gates and noisy ancillas, *Phys. Rev. A* **71**, 022316 (2005).
  - [67] K. Bu and D. E. Koh, Efficient classical simulation of clifford circuits with nonstabilizer input states, *Phys. Rev. Lett.* **123**, 170502 (2019).
  - [68] E. T. Campbell, Catalysis and activation of magic states in fault-tolerant architectures, *Phys. Rev. A* **83**, 032317 (2011).
  - [69] A. Gu, S. F. E. Oliviero, and L. Leone, Doped stabilizer states in many-body physics and where to find them, *Phys. Rev. A* **110**, 062427 (2024).
  - [70] A. Gu, S. F. Oliviero, and L. Leone, Magic-induced computational separation in entanglement theory, *PRX Quantum* **6**, 020324 (2025).
  - [71] A. Gu, H.-Y. Hu, D. Luo, T. L. Patti, N. C. Rubin, and S. F. Yelin, Zero and finite temperature quantum simulations powered by quantum magic, *Quantum* **8**, 1422 (2024).
  - [72] M. Howard and E. Campbell, Application of a resource theory for magic states to fault-tolerant quantum computing, *Phys. Rev. Lett.* **118**, 090501 (2017).
  - [73] Z.-W. Liu and A. Winter, Many-body quantum magic, *PRX Quantum* **3**, 020333 (2022).
  - [74] J. R. Seddon, B. Regula, H. Pashayan, Y. Ouyang, and E. T. Campbell, Quantifying quantum speedups: Improved classical simulation from tighter magic monotones, *PRX Quantum* **2**, 010345 (2021).
  - [75] S. True and A. Hama, Transitions in entanglement complexity in random circuits, *Quantum* **6**, 818 (2022).
  - [76] M. Yoganathan, R. Jozsa, and S. Strelchuk, Quantum advantage of unitary clifford circuits with magic state inputs, *Proceedings of the Royal Society A: Mathematical, Physical and Engineering Sciences* **475**, 20180427 (2019).

- [77] S. Zhou, Z.-C. Yang, A. Hamma, and C. Chamon, Single T gate in a Clifford circuit drives transition to universal entanglement spectrum statistics, *SciPost Phys.* **9**, 087 (2020).
- [78] M. Bejan, C. McLauchlan, and B. Béri, Dynamical Magic Transitions in Monitored Clifford+T Circuits, (2023), [arXiv:2312.00132 \[quant-ph\]](#).
- [79] D. E. Koh, Further extensions of clifford circuits and their classical simulation complexities, *Quantum Information and Computation* **17**, 262–282 (2017).
- [80] A. Bouland, J. F. Fitzsimons, and D. E. Koh, Complexity classification of conjugated clifford circuits (Schloss Dagstuhl – Leibniz-Zentrum für Informatik, 2018).
- [81] Y. Zhang and Y. Gu, *Quantum magic dynamics in random circuits* (2024), [arXiv:2410.21128 \[quant-ph\]](#).
- [82] D. Qian and J. Wang, Quantum nonlocal nonstabilizerness, *Phys. Rev. A* **111**, 052443 (2025), [arXiv:2502.06393 \[quant-ph\]](#).
- [83] A. Ahmadi and E. Greplova, Quantifying non-stabilizerness via information scrambling, *SciPost Phys.* **16**, 043 (2024), [arXiv:2204.11236 \[quant-ph\]](#).
- [84] R. Wagner, F. C. R. Peres, E. Z. Cruzeiro, and E. F. Galvão, Certifying nonstabilizerness in quantum processors, (2024), [arXiv:2404.16107 \[quant-ph\]](#).
- [85] D. A. Korbany, M. J. Gullans, and L. Piroli, Long-range nonstabilizerness and phases of matter, (2025), [arXiv:2502.19504 \[quant-ph\]](#).
- [86] E. Tirrito, P. S. Tarabunga, G. Lami, T. Chanda, L. Leone, S. F. E. Oliviero, M. Dalmonte, M. Collura, and A. Hamma, Quantifying nonstabilizerness through entanglement spectrum flatness, *Phys. Rev. A* **109**, L040401 (2024), [arXiv:2304.01175 \[quant-ph\]](#).
- [87] X. Turkeshi, M. Schirò, and P. Sierant, Measuring nonstabilizerness via multifractal flatness, *Phys. Rev. A* **108**, 042408 (2023), [arXiv:2305.11797 \[quant-ph\]](#).
- [88] S. Cusumano, L. C. Venuti, S. Cepollaro, G. Esposito, D. Iannotti, B. Jasser, J. O. c, M. Viscardi, and A. Hamma, Non-stabilizerness and violations of CHSH inequalities (2025), [arXiv:2504.03351 \[quant-ph\]](#).
- [89] P. Sierant, P. Stornati, and X. Turkeshi, *Fermionic magic resources of quantum many-body systems* (2025), [arXiv:2506.00116 \[quant-ph\]](#).
- [90] J. Odavic, M. Viscardi, and A. Hamma, Stabilizer entropy in nonintegrable quantum evolutions, *Phys. Rev. B* **112**, 104301 (2025).
- [91] M. Włodarczyk, P. Caban, J. Ciborowski, M. Drakowski, and J. Rembielinski, Quantum spin correlations in Moller scattering of relativistic electron beams, *Phys. Rev. A* **95**, 022103 (2017).
- [92] P. Caban, J. Rembielinski, and M. Włodarczyk, Einstein-Podolsky-Rosen correlations of vector bosons, *Phys. Rev. A* **77**, 012103 (2008).
- [93] C. Cao, *Non-trivial area operators require non-local magic* (2024), [arXiv:2306.14996 \[hep-th\]](#).
- [94] V. G. J. Stoks, R. A. M. Klomp, C. P. F. Terheggen, and J. J. de Swart, Construction of high-quality nn potential models, *Phys. Rev. C* **49**, 2950 (1994).
- [95] R. Klomp, J. de Swart, T. Rijken, C. Terheggen, R. Timmermans, V. Stoks, J. Rubio-Melón, and W. Vink, *NN-online*, <https://nn-online.org/nn/> (2024).
- [96] J. Benesch *et al.* (MOLLER), The MOLLER Experiment: An Ultra-Precise Measurement of the Weak Mixing Angle Using Moller Scattering, (2014), [arXiv:1411.4088 \[nucl-ex\]](#).
- [97] *The MOLLER Experiment* (2025).
- [98] M. Blasone, S. D. Siena, G. Lambiase, C. Matrella, and B. Micciola, *Complete complementarity relations in tree level qed processes* (2024), [arXiv:2402.09195 \[quant-ph\]](#).
- [99] Wolfram Research, Inc., *Mathematica, Version 14.3*, Champaign, IL, 2025.

### Appendix A: Measurements for Estimating Anti-Flatness

For a two-particle final state, the reduced density matrix corresponds to a  $2 \times 2$  matrix that, in spin-space, can be reconstructed from expectation values of the spin operator along (any) three cartesian axes,

$$\rho_A = \frac{1}{2} \sum_i \langle \bar{\sigma}_i \rangle_A \bar{\sigma}_i, \quad (\text{A1})$$

where  $\langle \bar{\sigma}_i \rangle_A = \text{Tr}(\hat{\rho}_A \bar{\sigma}_i)$ . Measuring the spin components of one of the final state particles, provides an estimator for  $\rho_A$  from Eq. (A1), and hence an estimator for the anti-flatness using Eq. (6).

### Appendix B: Two-qubit Stabilizer States

For two qubits (with  $d = 4$ ), there are four stabilizer operators for each of the sixty stabilizer states given in Table I. Thirty-six of these states are tensor products formed from one-qubit stabilizers, while the remaining twenty-four are entangled states.

state	$ 00\rangle$	$ 01\rangle$	$ 10\rangle$	$ 11\rangle$	state	$ 00\rangle$	$ 01\rangle$	$ 10\rangle$	$ 11\rangle$
1	1	1	1	1	37	0	1	1	0
2	1	-1	1	-1	38	1	0	0	-1
3	1	1	-1	-1	39	1	0	0	1
4	1	-1	-1	1	40	0	1	-1	0
5	1	1	i	i	41	1	0	0	i
6	1	-1	i	-i	42	0	1	i	0
7	1	1	-i	-i	43	0	1	-i	0
8	1	-1	-i	i	44	1	0	0	-i
9	1	1	0	0	45	1	1	1	-1
10	1	-1	0	0	46	1	1	-1	1
11	0	0	1	1	47	1	-1	1	1
12	0	0	1	-1	48	1	-1	-1	-1
13	1	i	1	i	49	1	i	1	-i
14	1	-i	1	-i	50	1	i	-1	i
15	1	i	-1	-i	51	1	-i	1	i
16	1	-i	-1	i	52	1	-i	-1	-i
17	1	i	i	-1	53	1	1	i	-i
18	1	-i	i	1	54	1	1	-i	i
19	1	i	-i	1	55	1	-1	i	i
20	1	-i	-i	-1	56	1	-1	-i	-i
21	1	i	0	0	57	1	i	i	1
22	1	-i	0	0	58	1	i	-i	-1
23	0	0	1	i	59	1	-i	i	-1
24	0	0	1	-i	60	1	-i	-i	1
25	1	0	1	0					
26	0	1	0	1					
27	1	0	-1	0					
28	0	1	0	-1					
29	1	0	i	0					
30	0	1	0	i					
31	1	0	-i	0					
32	0	1	0	-i					
33	1	0	0	0					
34	0	1	0	0					
35	0	0	1	0					
36	0	0	0	1					

TABLE I. The complete set of sixty two-qubit stabilizer states. For notational purposes, we identify  $|0\rangle = |\uparrow\rangle$  and  $|1\rangle = |\downarrow\rangle$ . The left set are from the tensor product of one-qubit stabilizer states, while the right set are entangled states. They are (generally) unnormalized, and require coefficients of either 1 or  $\frac{1}{\sqrt{2}}$  or  $\frac{1}{2}$ .

### Appendix C: More Details on Low-Energy NN Scattering

For NN scattering, the stabilizer states separate into three distinct groups, where the states in each group lead to the same total linear magic in the outgoing states:

$$\text{Group 1} = \begin{cases} 1, 4, 17, 20, 33, 36 \text{ (tensor products)} \\ 37 \rightarrow 41, 44, 45, 48, 57, 60 \text{ (entangled)} \end{cases} \quad (\text{C1})$$

$$\text{Group 2} = \begin{cases} 2, 3, 18, 19, 34, 35 \text{ (tensor products)} \\ 42, 43, 46, 47, 58, 59 \text{ (entangled)} \end{cases} \quad (\text{C2})$$

$$\text{Group 3} = \begin{cases} 5 \rightarrow 16 \text{ and } 21 \rightarrow 32 \text{ (tensor products)} \\ 49 \rightarrow 56 \text{ (entangled)} \end{cases} \quad (\text{C3})$$

Fig. 5 shows the full linear magic  $\mathcal{M}_{\text{lin}}(\hat{S}|\psi_i\rangle)$ , linear entanglement entropy and non-local magic (here equivalent to anti-flatness) for outgoing states in NN scattering resulting from tensor-product and entangled initial states  $|\psi_i\rangle$  from groups 1, 2 and 3.

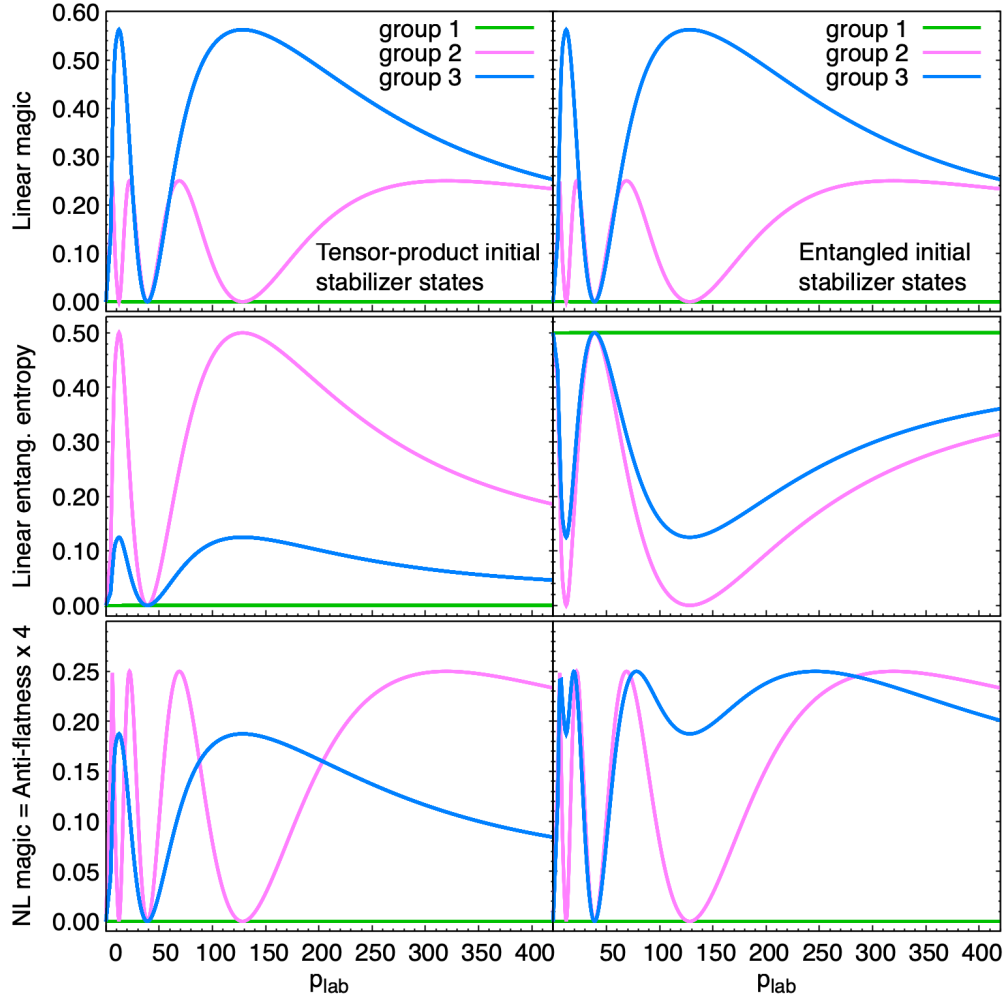


FIG. 5. Total linear magic (top), linear entanglement entropy (middle), and non-local linear magic (anti-flatness  $\times 4$ ) in NN scattering. The left (right) panels show the results for outgoing states from initial unentangled (entangled) stabilizer states.

While the total magic produced is the same for tensor-product and entangled initial states within each group, the fluctuations in entanglement differ for group-3. Specifically it is seen that, in this group, the interaction dis-entangles more effectively than it entangles. This results in non-local magic (or anti-flatness) patterns exhibiting more structure when the initial states are entangled. This is not the case for states of group-2 for which the dis-entangling power is about the same as the entangling power.

### Appendix D: More Details on High-Energy Møller Scattering

We choose to use the helicity-amplitude parameterization of the scattering amplitude, with expressions given in Ref. [1, 2], and not the computational basis used in Ref. [56]. However, given the basis independence of anti-flatness and non-local magic, either basis could have been chosen. The helicity amplitudes that are non-zero in the high-energy limit (or  $m_e \rightarrow 0$ ), in terms of Mandelstam variables, are [1, 2] (neglecting factors of  $e^2$ , the electromagnetic coupling constant)

$$\begin{aligned} A_{RR:RR} &= A_{LL:LL} = -\frac{2(t+u)^2}{tu}, \\ A_{RL:RL} &= A_{LR:LR} = -\frac{2u}{t}, \\ A_{RL:LR} &= A_{LR:RL} = +\frac{2t}{u}. \end{aligned} \quad (D1)$$

They can be written in terms of the center-of-momentum scattering kinematics,

$$\begin{aligned} p_1 &= (E/2, 0, 0, |\mathbf{p}_e|), \quad p_2 = (E/2, 0, 0, -|\mathbf{p}_e|), \\ p_3 &= (E/2, 0, |\mathbf{p}_e| \sin \theta, |\mathbf{p}_e| \cos \theta), \quad p_4 = (E/2, 0, -|\mathbf{p}_e| \sin \theta, -|\mathbf{p}_e| \cos \theta), \\ |\mathbf{p}_e|^2 &= (E/2)^2 + m_e^2, \\ s &= (p_1 + p_2)^2, \quad t = (p_1 - p_3)^2, \quad u = (p_1 - p_4)^2, \\ s &= E^2, \quad t = -2|\mathbf{p}_e|^2(1 - \cos \theta), \quad u = -2|\mathbf{p}_e|^2(1 + \cos \theta), \end{aligned} \quad (D2)$$

where  $\theta$  is the scattering angle in the center of momentum.

For Møller scattering, the stabilizer states contributing to the final state magic separate into five distinct groups:

$$\text{Group 1} = \begin{cases} 33, 36 \text{ (tensor products)} \\ 37 \rightarrow 41, 44 \text{ (entangled)} \end{cases} \quad (D3)$$

$$\text{Group 2} = \begin{cases} 1, 4, 17, 20 \text{ (tensor products)} \\ 45, 48, 57, 60 \text{ (entangled)} \end{cases} \quad (D4)$$

$$\text{Group 3} = \begin{cases} 2, 3, 18, 19 \text{ (tensor products)} \\ 46, 47, 58, 59 \text{ (entangled)} \end{cases} \quad (D5)$$

$$\text{Group 4} = \begin{cases} 34, 35 \text{ (tensor products)} \\ 42 \text{ (entangled)} \end{cases} \quad (D6)$$

$$\text{Group 5} = \begin{cases} 5 \rightarrow 16 \text{ and } 21 \rightarrow 32 \text{ (tensor products)} \\ 49 \rightarrow 56 \text{ (entangled)} \end{cases} \quad (D7)$$

We find that the tensor-product states within each Group-1,2,3,4 display the same anti-flatness. However tensor-product states in Group-5 do not. Hence, we further sub-divide the tensor-product states in Group-5 into two sub-groups,

$$\begin{aligned} \text{Group} - 5a &= 5, 6, 7, 8, \text{ and } 13, 14, 15, 16, \\ \text{Group} - 5b &= 9, 10, 11, 12, \text{ and } 21 \rightarrow 32. \end{aligned} \quad (D8)$$

Fig. 6 shows the full linear magic, linear entanglement entropy and non-local magic (here equivalent to anti-flatness) for outgoing states in Møller scattering  $|\chi_i\rangle = \mathcal{N}\hat{\mathcal{A}}|\psi_i\rangle$  resulting from tensor-product and entangled initial states  $|\psi_i\rangle$  from groups 1-5. It is interesting to note that the entanglement entropy is maximal at  $\theta = \pi/2$  for all groups, and for the average value, consistent with the observations in Ref. [1, 2], while this is not the case for the magic.

In contrast to the strong nuclear force in NN scattering, we observe a large asymmetry between the entanglement and dis-entanglement power in the present quantum electrodynamics process. In particular the interaction is not able to decrease the entanglement of maximally-entangled initial states, which results in no non-local magic (or anti-flatness) being produced. Thus in this case the generated magic is entirely local, meaning that the outgoing states remain entangled stabilizer states in a different local basis.

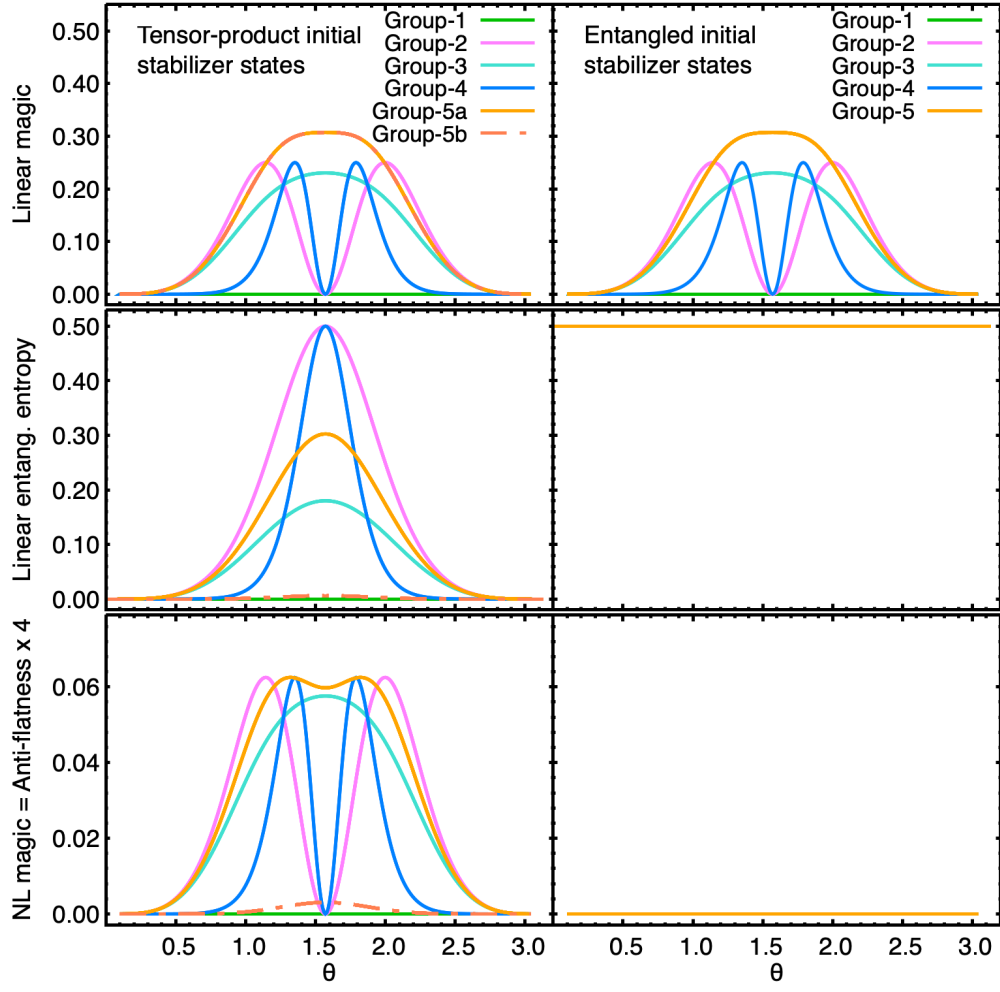


FIG. 6. Total linear magic (top), linear entanglement entropy (middle), and non-local linear magic (anti-flatness  $\times 4$ ) in Møller scattering. The left (right) panels show the results for outgoing states from initial unentangled (entangled) stabilizer states.